Aerothermodynamic Assessment of Conceptual and Detail Configuration Changes to a Rocket Propelled Aircraft

Jack A. Griffin[1]
Timothy T. Takahashi[2]
Arizona State University, Tempe, AZ, 85281, US
and
Patrick E. Rodi[3]
William Marsh Rice University, Houston, TX, 77251, US

In order to configure a successful high Mach Number aircraft for flight through the Earth's atmosphere, designers must consider aerothermodynamic effects. The mission thermal response of a hypersonic aircraft is a function of its flight profile as well as nuance in sweep angles, leading edge radii and materials thicknesses. Small changes in these design parameters may enable or preclude the inclusion of common aerospace materials (such as heat-treated aluminums, titaniums or stainless steels) which lead to large changes in structural weight and internal design. Since "everything affects everything" in aircraft design, engineers need to understand how the mission thermal response changes as a result of these decisions. This paper demonstrates the parametric study utility of a coupled aerothermal / kinematic performance "Mission Code" as applied to flown and proposed derivatives of the North American X-15 rocket plane.

Nomenclature

ALT	=	altitude, ft
C_D	=	coefficient of drag
C_L	=	coefficient of lift
C_p	=	pressure coefficient, $((p-p_\infty)/q_\infty)$
C_{pmax}	=	pressure coefficient after normal shock
c_p	=	specific heat capacity, BTU/lbm-°R
c_f	=	compressible skin-friction coefficient
c_{f0}	=	incompressible skin-friction coefficient
h	=	specific enthalpy, BTU/lbm
K	=	hypersonic similarity parameter
k	=	thermal conductivity, BTU/ft-hr-°R
M	=	Mach Number
n	=	mesh time index
p	=	pressure, lbf/ft^2
Pr	=	Prandtl Number
q	=	dynamic pressure, lbf/ft^2
$\dot{q}$	=	heat transfer, BTU/ft^2-hr
R	=	nose radius, ft
Re	=	Reynolds Number
S_{ref}	=	aerodynamic reference area, ft^2
St	=	Stanton number
T	=	temperature, °R
t	=	time, s
U	=	velocity, ft/s
Z	=	compressibility factor
x	=	position in mesh, ft
α	=	angle of attack, deg
β	=	$\sqrt{M_\infty^2 - 1}$
γ	=	ratio of specific heats
θ	=	turning angle, deg
ε	=	emissivity
κ	=	thermal diffusivity, ft^2/sec
Λ	=	leading edge sweep, deg
μ	=	dynamic viscosity, slug/(ft-sec)
ρ	=	air density, slug/ft^3
σ	=	Stefan-Boltzmann constant, BTU/sec-ft^2-°R^4

Subscripts

aw	=	adiabatic wall
CO	=	circular orbit
e	=	boundary layer edge
SL	=	sea level

---

[1] M.S. Graduate – Aerospace Engineering, School for the Engineering of Matter, Transport and Energy, Arizona State University, Tempe, AZ, 85287.
[2] Professor of Practice – Aerospace Engineering, School for the Engineering of Matter, Transport and Energy, Arizona State University, Tempe, AZ, 85287. AIAA Associate Fellow.
[3] Professor in the Practice, Mechanical Engineering Department, George R. Brown School of Engineering, William Marsh Rice University, Houston, TX, 77251. AIAA Associate Fellow.

t	=	total (or stagnation) value
w	=	wall, surface value
∞	=	free stream

I. Introduction

HIGH-SPEED and HYPERSONIC aircraft fly in a challenging environment. Flight at high speeds are associated with operation at very high stagnation temperatures. Flight at high speeds and low altitudes are associated with operations at very high dynamic pressures; whereas flight at high speeds and very high altitudes are associated with operation at very low dynamic pressures in a rarefied atmosphere. The aerothermodynamic response of such an aircraft in flight is thus tremendously impacted by both the environment (things like stagnation temperature) as well as the ability for convective heat-transfer to transmit heat into (or out of) the airframe. Thus, an aircraft immersed in a very high temperature flow field with poor convection can easily be cooler than an aircraft immersed in a somewhat cooler flow field but with more effective convection. Similarly, the heat capacity of structure is equally important: thin sheet metal will prove more susceptible to follow the temperature profile of the local flow field than a thick forged part. All taken together, detail thicknesses of materials, sweep angles and leading-edge radii have a huge impact of the viability of a particular engineering material to survive hypersonic flight.

Consider the Space Shuttle Orbiter, a re-usable Hypersonic Aircraft designed to withstand the full thermal load of atmospheric re-entry for low-earth orbit; see FIGURE 1. Engineers selected a mix of aluminum and graphite reinforced epoxy to build the underlying airframe; thus the "buried" structure must remain "cold" and not exceed 350^{o}F over the course of the mission. [1] What makes the Orbiter interesting is that the entire structure is insulated from the external environment by a collection of differing thermal protection materials. Engineers employed Carbon-Carbon (with a 2700^{o}F limit) at the nose and across much of the wing outboard leading edge. Lighter weight "Shuttle Tile," HRSI, was employed over the whole underside, in the region of the wing inboard leading edge and in select places on the forebody. Much of the rest of the fuselage and leeward side of the wing is insulated with the Nomex felt, FRSI, which has only a 700^{o}F limit. While the basic airframe geometry and flight profiles define the thermal environment, the tailored selection of insulating materials successfully keep the primary structure cool and intact.

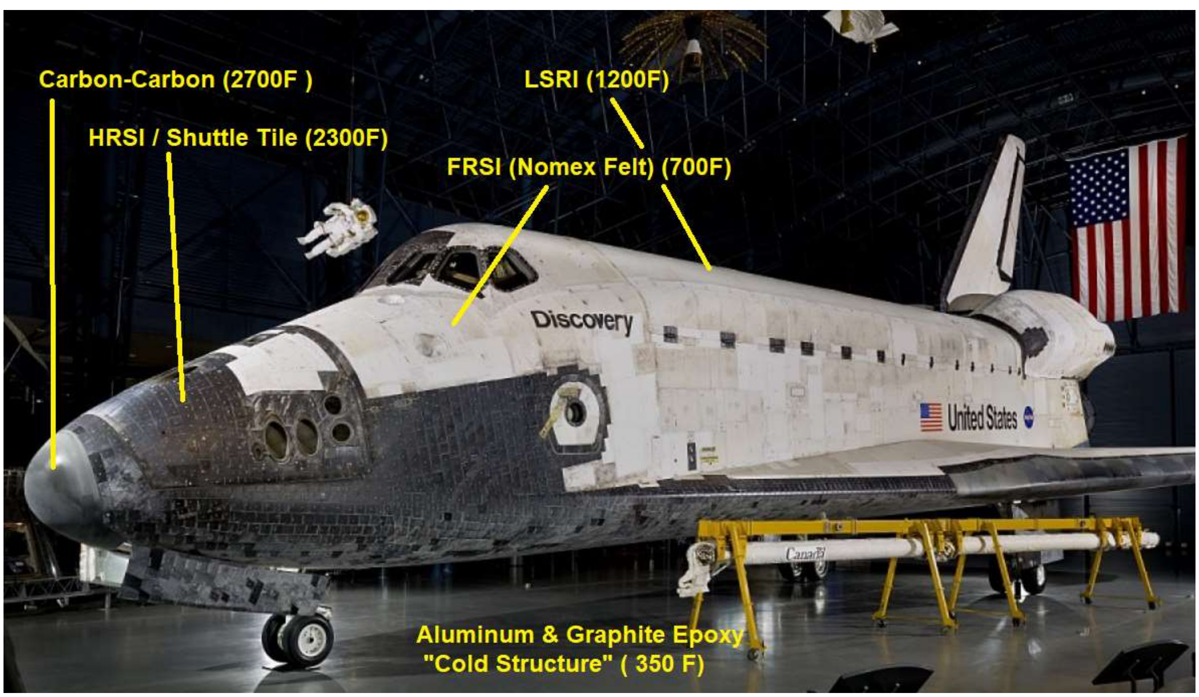

FIGURE 1 – Example Space Shuttle Orbiter – local tailoring of insulating materials

Future high-speed and hypersonic aircraft will need to express similar nuance in internal and external design. The materials selection will be a function both of the basic shape (what it looks like) as well as the expected trajectory (how it is flown). As the flight duration and peak Mach Number increases, the TPS weight and cost become an increasing percentage of the vehicle's total weight. Thus, aerothermodynamic considerations should be included as early in the design process as practicable. A modern, Model-Based-Systems-Engineering (MBSE) Multi-Disciplinary-Optimization (MDO) process should be well equipped with a tool to evaluate how large-scale and small-scale shape changes impact the trajectory, and thus the resulting thermal response.

Since "everything effects everything" in Aircraft Design, Materials selection strategies become "all-or-nothing" sorts of responses in an MDO trade study environment. The typical MDO logic flow will have the configuration master executive specify a geometry and a given materials strategy; see FIGURE 2. From there, aerodynamic and mass properties data can be inferred. Since the aerothermal response is driven by mission kinematics which are, in turn, driven by weight, aerodynamics and propulsion it is hard to envision any other decomposition of the design process. Therefore, the MDO framework can basically return a "pass / marginal / fail" verdict on a proposed vehicle / materials / trajectory strategy.

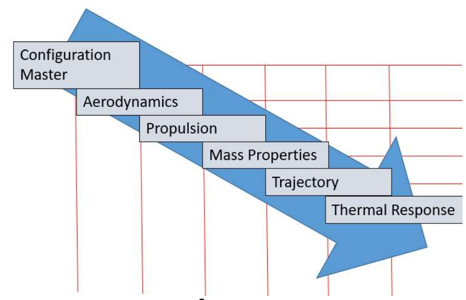

FIGURE 2 – N^2 DIAGRAM of MDO process for an Aerothermally Tailored Vehicle Design Study

In our previous two papers [2][3], we discussed the development of an extended Aircraft Style "Mission Code," with enhancements to accurately model hypersonic and exo-atmospheric flight and to provide aerothermal estimates for a reasonable number of control points. It showcases a "computationally lean" tool that can support a wide ranging MDO effort.

The Mission Analysis techniques have been used to generate successful aircraft designs for decades, and can help avoid the need for resource intensive 3DOF and/or 6DOF analysis or delays the use of such tools until much later in the development program. Examples of such Mission Analysis programs include NSEG [4][5][6][7], and Professor Takahashi's Mission Code which we use as the basis for this work.[8][9][10][11] Aspects of the computer program's development, such as mission segment definitions and analysis, aerodynamic, mass properties, and propulsion, are described in "Aero-Spaceplane Mission Performance Estimations Incorporating Atmospheric Control Limits," by Griffin & Takahashi.[2] Details of the Aerothermal Model are described in another companion paper, "Aerothermodynamic Modeling for a "Mission Code" Approach to Hypersonic Flight," by Griffin, Takahashi and Rodi. [3]

II. Methods for Calculating the Flight Path

Engineers typically simulate low-speed aircraft payload/range performance using a time-step integrating point-mass simulation, known as a "mission code." These programs, utilizing "trimmed" aerodynamics data, speed/altitude/throttle dependent propulsion data and basic mass properties, capture the flight path of an aircraft in the absence what are classically considered "inner loop" control laws and, instead, utilize commands and directives that pilots and air traffic controllers are familiar with.

A. KINEMATIC PERFORMANCE MODEL

The core "mission code" is a time-step integrating algorithm that explicitly defines maneuvers such as "climb at constant knots equivalent airspeed" (*KEAS)*, "acceleration at constant altitude," "maintain steady level flight," etc. Then at each integration step the code takes the explicitly defined state variables such as power lever angle (*PLA*) and computes the implicit simulation variable such as the current weight, altitude (*ALT*), flight path angle, rate of climb (R.O.C.), etc. Written in EXCEL/VBA, the code employs three input datasets: trimmed aerodynamic performance data, "five-column" propulsion performance data, and a mission profile file. The code produces time or distance history plots of a host of parameters such as dynamic pressure, *KEAS*, angle-of-attack, dimensional lift, dimensional drag, *L/D* ratio and others. Due to its integration with EXCEL the data can be easily exported to MDO trade study environments, such as *ModelCenter*.

The aero performance data consist of tables of trimmed lift coefficient $C_L(M, \alpha)$ and trimmed drag coefficient $C_D(M, \alpha)$ at a reference altitude as well as Reynolds Numbers based corrections to drag $\Delta C_D(M, ALT)$. The fundamental tables are fully populated, and amenable for interpolation.

The propulsion five column data, as the name suggests, comprise fully populated tables of thrust and thrust specific fuel consumption (*TSFC*) as a function of flight Mach Number, altitude and *PLA*.

The code forms a mission profile from a sequence of mission segments. These segments are defined in a human readable text file that contain phrases common to pilots and air traffic controllers, known as "Pilot Talk"; see TABLE 1. A typical hypersonic flight of an air launched vehicle would begin at a specified weight, speed and altitude. The mission would begin with a ballistic air drop followed by engine start and powered flight. The aircraft may fly at constant airspeed (or dynamic pressure) or Mach number (excess thrust would cause the aircraft to climb), constant altitude (excess thrust would cause the aircraft to accelerate), or constant angle-of-attack or lift coefficient (excess thrust will cause the aircraft to accelerate/climb). These commands allow the mission planner to prescribe the trajectory in a manner consistent with other performance data as found in an aircraft flight manual; see FIGURE 3.

TABLE 1 Example Mission Profile

Segment	Condition
0→1	M = 0.8, ALT = 45000-ft, PLA = 0, Constant α = 0°, Until ALT < 43,000-ft
1→2	PLA = 1, Constant α = 12°, Until ALT > 43,000-ft
2→3	Constant α = 8°, Until M > 2.5
3→4	Constant α = 2°, Until M > 3, then cutoff motor
4→5	PLA = 0, Constant α = 5°, Deploy Drag Brake Until ALT < 60,000-ft
5→6	Constant α = 8°, Until ALT < 50,000-ft
6→	Constant α = 5°, Until ALT < 40,000-ft

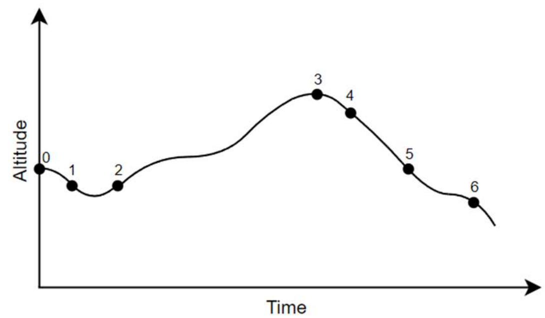

FIGURE 3 – Example Trajectory as defined by "Pilot Talk" showing the segment described in TABLE 1

III. Methods for Calculating Aerothermal Heating

The aerothermodynamic model used is detailed enough to provide concrete data on the suitability of a proposed materials / thermal protection-system (TPS) strategy for a proposed vehicle. In the following section, the equations and algorithms presented are used to predict the aerodynamic heating to leading edges and acreage regions of the vehicle. Importantly models showcased in this were selected to provide a "computationally lean" method to generate engineering-level estimates of the thermal history of high-speed vehicle regions for the supersonic to low hypersonic Mach regime (M ≤ 8).

A. GEOMETRY INDEPENDENT AEROTHERMAL PARAMETERS

The trajectory dependent and geometry independent characteristics are found below. Starting with the 1976 Standard Atmosphere [12], an estimate of freestream ambient conditions is recorded along the trajectory. Using Mach number and altitude along the trajectory the dynamic pressure can be found as the mission is flown. Similarly, the stagnation temperature can be derived as the Mach number is known throughout the flight, the total-to-static relation is used see below:

$$T_t = T\left(1 + \frac{\gamma - 1}{2} M^2\right) \tag{1}$$

A common parameter tracked is a reference heating rate, which is typically done using a 1-ft radius reference sphere. The reference heating rate for a notional 1-ft radius sphere was extensively used in the X-15, Space Shuttle Orbiter, and many other hypersonic vehicle development programs. The method used here to calculate the heating rate, as reported by Bertin [13], is the Detra Stagnation Point correlation for hemispherical noses. This method uses a simple correlation for the stagnation point conductive heating rate. These correlations begin by predicting the conductive heating rate in BTU/ft^2-s to the stagnation point of a sphere of a given nose radius, R:

$$\dot{q}_{spher} = \frac{17600}{\sqrt{R}} \left(\frac{\rho_\infty}{\rho_{SL}}\right)^{0.5} \left(\frac{U_\infty}{U_{CO}}\right)^{3.15} \tag{2}$$

where the freestream and sea level densities are ρ_∞ and ρ_{SL}, respectively, and the freestream and circular orbit velocities are U_∞ and U_{CO}, respectively.

B. GEOMETRY DEPENDENT AEROTHERMAL PARAMETERS

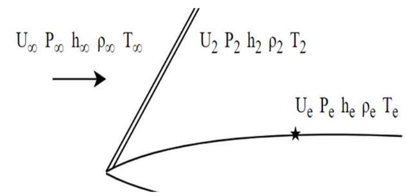

FIGURE 4 – Wall Conditions at the edge are a function of upstream flowfield

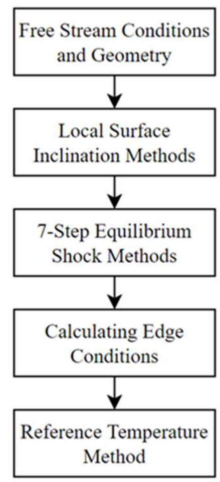

FIGURE 5 – Aerothermodynamic Process

Since real hypersonic aircraft are not 1-ft radius spheres, we must also predict stagnation temperatures and stagnation point heating rates on realistic geometries.

For the leading edge of wings and stabilizers the heating is done by modifying the stagnation point heating rate estimate for the hemisphere, $\dot{q}_{spher}$, to the heating rate on an unswept cylinder by dividing the spherical rate by $\sqrt{2}$: $\dot{q}_{cylinder} = \frac{\dot{q}_{sphere}}{\sqrt{2}}$. This value is then multiplied by the product *cos(Λ)cos(α)* to find the stagnation point heating rate for an arbitrary swept cylinder; where *Λ* is the leading-edge sweep and *α* is the angle of attack.[31] The resulting heating rate is used for leading edge on wings.

$$\dot{q}_{LE} = \frac{17600}{\sqrt{2}\sqrt{R}} \left(\frac{\rho_\infty}{\rho_{SL}}\right)^{0.5} \left(\frac{U_\infty}{U_{CO}}\right)^{3.15} cos(\Lambda)\, cos(\alpha) \tag{3}$$

To determine the heating rate at other locations the code uses the Reference Temperature Method to predict the local skin friction coefficient for the boundary layer. Then knowing the local compressible skin friction, we use the engineering approach called the "Reynolds Analogy." This relates the local skin friction to the Stanton number, *St*. The Stanton number can then be used to predict the heating rate. A more detailed explanation of this process can be found in the aerothermal companion paper. [3] The Reference Temperature method needs to know properties at the edge of the boundary condition. To predict the edge temperature and other gas properties requires downstream some insight into to the flow history upstream is needed, see FIGURE 4. To find the edge values, the code follows the procedure shown in FIGURE 5. Each physical point of interest must be defined in terms of its local inclination to the freestream direction. From this, we may find the static pressure using a local inclination method and by using shock relations to determine the total pressure. Isentropic relations can be used to find the remaining unknowns at the boundary layer edge.

The method treats the points as inclined plates. The angle of these plates is the result of the cross product of the normal vector of the surface of interest with that of the oncoming freestream flow. Thus, the wing, horizontal tail, and fuselage acreage points depend on the summation of the flight angle of attack and the local inclination of the surface feature. Conversely, the vertical tail's local inclination would be dependent on the local geometry and side slip. In practice the local geometry is simply an offset added to the angle of attack or side slip.

The code estimates the conditions after the shock using one of two methods. When the oncoming flow $M <= 3$, we use the equations from NACA Report 1135, [14]. When the oncoming flow $M > 3$, we deem the shock sufficiently strong to need to consider thermally perfect conditions or chemically reacting mixture conditions. Thus, the algorithm will substitute Mollier charts, [15] in lieu of the calorically perfect relationships. Mollier tables define total temperature (T_t), Z, and γ as a function of enthalpy and static pressure.

Once the code finds post shock conditions, whether by calorically perfect, thermally perfect or chemically reacting methods, it can then solve for the conditions behind the shock using Anderson's "Seven-Step Iterative Method".[16]

This method uses the Mach Number at the local boundary edge condition relevant to heating to obtain the total pressure at the edge, P_{te}, then uses the local inclination method to obtain the static pressure at the edge, P_e:

$$\frac{P_{te}}{P_e} = \left(1 + \frac{\gamma - 1}{2} M_e{}^2\right)^{\frac{\gamma}{\gamma - 1}} \tag{5}$$

The remaining edge values can be found using relations such as Sutherland's Law. [16]

C. COLD VS HOT WALLED STRUCTURES

Finally, for real Hypersonic Aircraft, the actual heat transfer rate will vary due to the aircraft's surfaces temperature. By assuming a Stanton number is approximately equal for both hot and cold wall conditions. The heating rate for the hot walled structure can be found.

For adiabatic surfaces the conduction into the structure is zero making the surface reach radiative equilibrium, where the heat in equals the heat radiated out.

$$\dot{q}_{w,hot} = \varepsilon \sigma T_{hot}^4 \quad (6)$$

If the surface is not well insulated, conduction into the surface results in significant changes in resulting surface temperature time history. The code uses a FTCS method to compute the temperature gradient across a given material and thickness. Here, the outer boundary condition is forced such that the gradient temperature plus the radiation out equals the conductive in. Whereas, the inner body boundary conditions are defined on an individual control point basis. This requires only a very rudimentary knowledge of the internal structure configuration. If the internal structure is a material that has a large thermal mass such as fuel, the solution algorithm employs a Dirichlet boundary condition where the inner surface equals the constant temperature of the thermal mass. Otherwise, the algorithm uses a Neumann approach to define an adiabatic boundary condition for hot structure designs or to impose a symmetry condition.

D. NEED FOR CONTROL POINTS

In order to avoid needing a fully define 3D model the code predicts thermal characteristics at a discrete number of "control points." The control points can be defined at locations of interest regions such as at the nose, wing and tail leading edges, the leeward centerline, and windward centerline, see FIGURE 6. The type of point defines the aerothermodynamic method(s) used. For example, a control point might include: 1) the vehicle nose with a defined hemispherical radius; 2) a leading edge with defined sweep and leading-edge radius, 3) regions on the windward or leeward centerline of the vehicle – which requires insight as to its distance downstream along a streamline and whether the control point exists behind a normal or oblique shock wave.

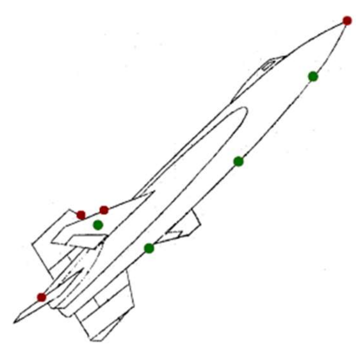

FIGURE 6 – Example Control Points on the North American X-15 Located in Regions of the Aircraft That Were Heavily Instrumented During the Test-flight Program. **RED** – Leading Edge; **GREEN** –acreage [17]

To quantify the thermal response of a vehicle component, we need to further define the emissivity, materials lay-up (thermal conductivity and thickness of various layers) as well as the boundary conditions applicable to any internal boundary (symmetry or heat sink). At each control point, the thermal stack consists of a user defined number of equally spaced nodes arrayed perpendicular to the surface. The initial temperature of the nodes is uniformly defined as the ambient temperature at the start of mission. The thermal diffusivity and thermal conductivity are user defined constants; the emissivity varies with temperature.

During the preliminary design process, engineers will conceptualize a thermal protection system strategy across the vehicle; the time history thermal response predictions from the aerothermal mission code will be used to determine if the design will withstand the expected aero-thermal environments. For the purposes of this paper, we use the North American X-15 geometry, aerodynamic, propulsion, and thermal models and place our control points at the locations instrumented on the actual flight test aircraft. Then compare the instrumented locations with the simulated and with the alternative configurations.

E. INTEGRATION INTO THE EXISTING MISSION PERFORMANCE CODE

The primary point-mass-simulation mission code operates on a 1-sec time step integration. Thus, as the aircraft moves along a trajectory the weight, flight Mach number, altitude and airframe attitude are updated at each time step. We compute the surface temperature time history in lockstep with the trajectory following the method shown in FIGURE 7. The 1976 Standard Atmosphere model defines the freestream environment at each time step. By looking at every control point using the known state variables, the code solves for the heating using either edge values and the Reference Temperature Method or using Detra's Stagnation Point Heating Correlation as governed by the geometry. Then the heating rate is used to calculate the surface temperature.

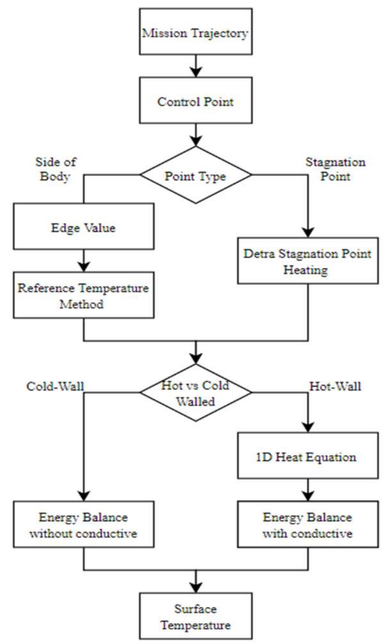

FIGURE 7 – Integration of Aerothermal Modeling into the Mission Code

TABLE 2: Material Properties of Inconel X

Thermal Diffusivity	$0.13\frac{ft^2}{hr}$
Thermal Conductivity	$89\frac{BTU\cdot in}{hr\cdot ft^{2}\cdot{}^{o}R}$
Emissivity	0.895 at 1060°R 0.925 at 2460°R

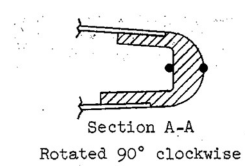

FIGURE 8 – Leading Edge Wing as Shown in NASA TM-468 [17]

FIGURE 9 – a) Baseline X-15 and b) Proposed X-15-A3 Delta Wing Configuration

IV. Trade Studies Using Modified X-15 Geometry

To show the capability of the aerothermal model some modifications to the assumed X-15 properties are made and then compared with. Details of the aerodynamic performance data used here are derived from a combination of flight test, empirical and vortex-lattice CFD sources. This is covered in greater detail in the companion papers; see Reference [2][3].

The propulsion data for the X-15's XLR99 engine has been compiled by Maher [18]. As a substitute for data on the XLR11 engine, the XLR99 performance has been scaled back to 30% power.

The baseline material properties are Inconel-X, see TABLE 2. The geometries of the various wing leading edge features may be related to the schematic shown as FIGURE 8.

For example, the X-15 program entertained the idea of a derivative configuration with a large, highly swept delta wing; see FIGURE 9. As sweep plays into the stagnation point heating it would be valuable for an engineer designing the TPS to know how this configuration changes the temperature time histories. In addition to change in sweep the delta wing shape would likely be modified to have a sharper leading edge for vortex lift reasons. Thus, two thermal trades are desired, one for where the leading edge of the wing is the same radius as the actual X-15 but now with significant sweep. Secondly a case with the delta wing's sweep with a smaller hemisphere LE radius. The changes to thickness, radius, and sweep for the wing leading edge trades are seen in TABLE 3, below.

TABLE 3: Geometry of the Baseline X-15 Geometry Along with Trade Study Perturbations

	Radius (-in)	Sweep (°)	Thickness (-in)
Baseline Wing LE	0.375	25.64	0.04
Delta Wing LE	0.375	77	0.04
Sharper Delta Wing LE	0.05	77	0.04
Baseline	0.375	25.64	0.04
Sharper	0.1875	25.64	0.04
Blunter	0.75	25.64	0.04
Thinner	0.375	25.64	0.02
Thinner and Sharper	0.1875	25.64	0.02
Thinner and Blunter	0.75	25.64	0.02
Thicker	0.375	25.64	0.08
Thicker and Sharper	0.1875	25.64	0.08
Thicker and Blunter	0.75	25.64	0.08

The thickness of the segments of the wing on the baseline X-15 were chosen to best match the actual temperature, in addition to being reasonable thicknesses for their respective locations. Over the next few pages, we will show baseline as well as sensitivity analysis to document the effect of modifying the thickness and radius of the modestly swept baseline configuration.

Additionally, the engineer would want to know the temperatures that would be expected if the delta wing was used instead. The thickness and chord length for these trades are seen in TABLE 4.

TABLE 4: Variations in Spanwise Thickness

	Skin Thickness Used (-in)	Chord Length (-ft)
Baseline Wing Root Segment	0.070	14.91
Baseline Wing Tip Segment	0.050	2.98
Thicker Wing Root Segment	0.080	14.91
Thinner Wing Tip Segment	0.040	2.98
Delta Wing Root Segment	0.070	36

Our trade studies attempt to match the X-15 flight profile described in NASA TM X-468. [17] This flight was well within the atmosphere at near hypersonic Mach number. The mission profile is detailed in TABLE 5 with the segments being shown in FIGURE 10.

FIGUREs 11 through 15 compare various predicted to flight test data. Once again, note that there is very good agreement between the model and flight test data in terms of time vs altitude Mach number, angle-of-attack, dynamic pressure, stagnation temperature plots.

TABLE 5 – Reference Mission Profile

Segment	Condition
0→1	M = 0.8, ALT = 45000-ft, PLA = 0, Constant α = 0°, Until t = 12-sec
1→2	PLA = 0.5, Constant α = 11°, Until t = 40-sec
2→3	PLA = 1, Constant α = 9°, Until t = 60-sec
3→4	PLA = 1, Constant α = 8°, Until t = 240-sec
4→5	PLA = 1, Constant α = 2°, Until t = 285-sec, then cutoff motor
5→6	PLA = 0, Constant α = 8°, Until t = 295-sec
6→7	PLA = 0, Constant α = 4°, Until t = 305-sec
7→8	PLA = 0, Level Decelerate Until M < 1.8
8→	PLA = 0, Descend at constant KIAS

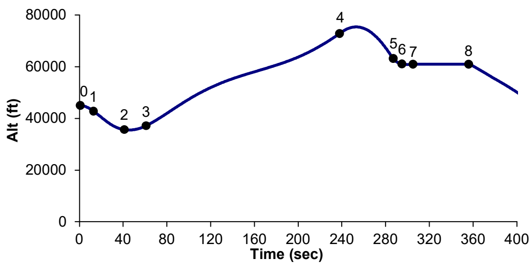

FIGURE 10 – NASA TM X-468 Trajectory

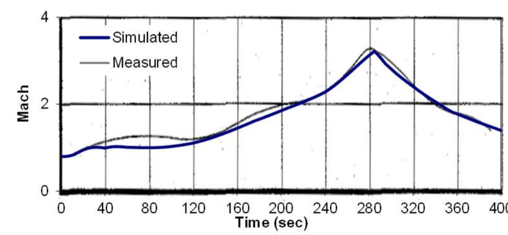

FIGURE 12 – Endo-Atmospheric Mission (Mach Number vs Time Comparison Between Simulation and Flight Test)

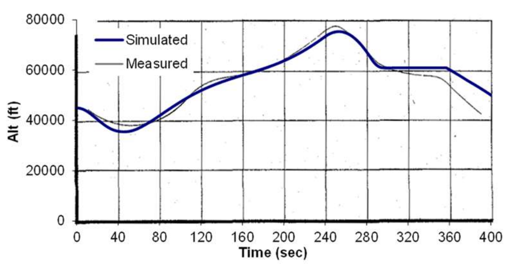

FIGURE 11 – Endo-Atmospheric Mission (Altitude vs Time Comparison Between Simulation and Flight Test)

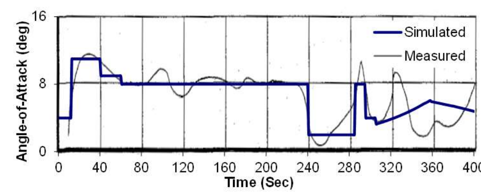

FIGURE 13 – Endo-Atmospheric Mission (Angle-of-Attack vs Time Comparison Between Simulation and Flight Test)

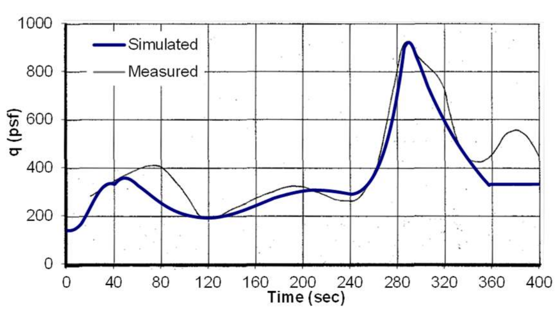

FIGURE 14 – Endo-Atmospheric Mission (Dynamic Pressure vs Time comparison between simulation and flight test)

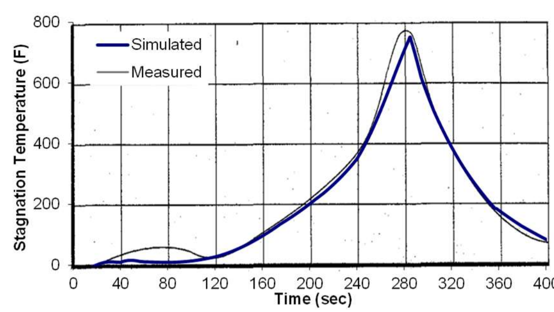

FIGURE 15 – Endo-Atmospheric Mission (Stagnation Temperature vs Time comparison between simulation and flight test)

For this flight, we compared the chordwise temperature distributions at different span locations at t = 308-sec in FIGUREs 16 through 18. To "best" match the data at the different sections, differing skin thicknesses were modelled. Because the wing is thin and essentially uncambered, the local inclination of the flow on the wing is dominated by the vehicle of attack. At the very leading edge of the wing, the local inclination is 10-degrees greater than the vehicle angle of attack. Mid-chord, the local inclination is the vehicle angle of attack. At the trailing edge, the local inclination is 5° less than the vehicle angle of attack.

The experimental data is given at t=308-sec because this time point represents the hottest point in the flight as described by NASA TM X-468. Note that peak stagnation temperatures occur at t~280-sec. Since the real airframe has some thermal inertia, peak vehicle temperatures tend to lag behind.

The thicker the skin, the cooler the temperatures. The leading edge was assumed to be a constant throughout the span. The general trend shows the temperature decreasing as the percentage along the chord increases. This is a factor of the geometry and the increasing Reynolds Number and simulated distributions track this tend well.

Near the side of body (FIGURE 16), windward surface temperatures are within 75°F and leeward surface temperatures are within 25°F using a skin thickness of 0.070-in.

Semi-span (FIGURE 17), windward surface temperatures are within 75°F and leeward surface temperatures are within 25°F using a skin thickness of 0.060-in.

Near the wing tip (FIGURE 18), windward surface temperatures are within 100°F and leeward surface temperatures are within 25°F using a skin thickness of 0.050-in.

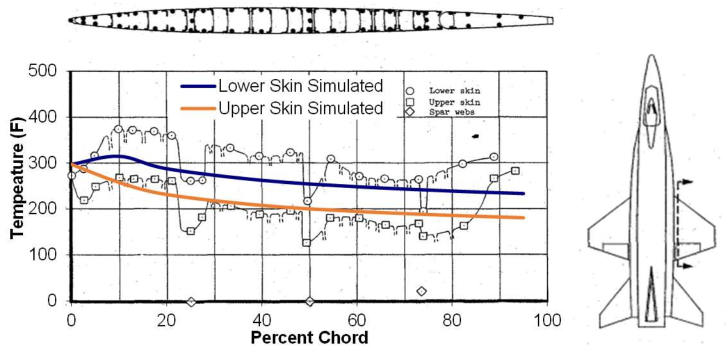

FIGURE 16 – Chordwise temperature distribution at t = 308-sec for the root section, baseline Skin thickness = 0.070-in

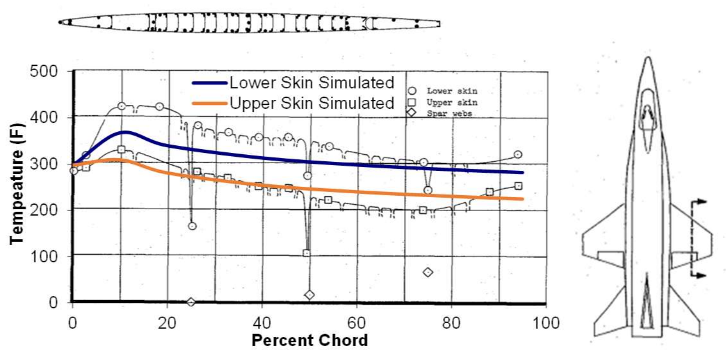

FIGURE 17 – Chordwise temperature distribution at t = 308-sec for the semispan section, baseline Skin thickness = 0.060-in

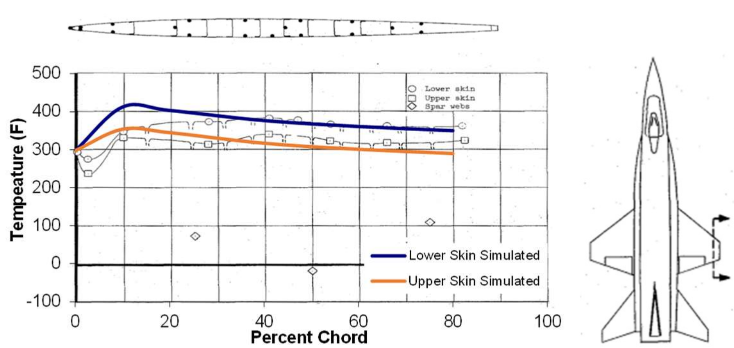

FIGURE 18 – Chordwise temperature distribution at t = 308-sec for the tip section, baseline Skin thickness = 0.050-in

Taken together, since our quasi-2D model does not differentiate spanwise positions along the wing, we can see how thickening the wing skins leads to a distinct decline in peak surface temparatures. Moving from 0.050-in to 0.070-in skins lowers the peak temperatures by nearly 100ºF.

To see how differing thicknesses and edge radii affect temperature, we developed further studies using the endo-atmospheric mission developed to match the instrumented flight described in NASA TM X-468.

To simplify matters, we kept the trajectory identical (i.e., we did not vary vehicle drag, lift or weights for these trades). As such, all differences in temperature are due to changes in leading edge radii, thickness, position, or sweep and not the trajectory.

FIGURE 19 shows that the increased sweep of the delta, 77°, reduces the temperature greatly. But by reducing the leading-edge radius from the initial 0.375-in to 0.050-in for the sharper LE case most of that temperature reduction is undone. This relation is to the engineer's benefit. A sharp leading edge is desired for heavily swept wings, which increases temperature, but this is counteracted by the reduction in heating caused by the reduced sweep of the delta wing. Thus, this highly swept configuration is feasible from a TPS perspective.

FIGURE 20 shows the change to the temperature as a result of modifying the thickness and radius of the leading edge of the wing. For this every combination of twice or half the thickness and radius is simulated. Notably there is a marked shift in the location of peak temperature with the thicker leading edges peaking first. Also, there is a +400°F difference between the thick/blunt combination over the thin/sharp combination. If this mission was the design case, then the massive difference in temperature between thick/blunt vs thin/sharp would necessitate different TPS strategies. If the thick/blunt LE was selected it would not be unreasonable for it to be made out of Aluminum opposed to the significantly more costly Inconel X.

The effect of the change in emissivity is small due to the relatively low temperatures (compared to re-entry). The baseline wing leading edge had an emissivity forced to different values resulting in FIGURE 21, where we see that the difference is negligible.

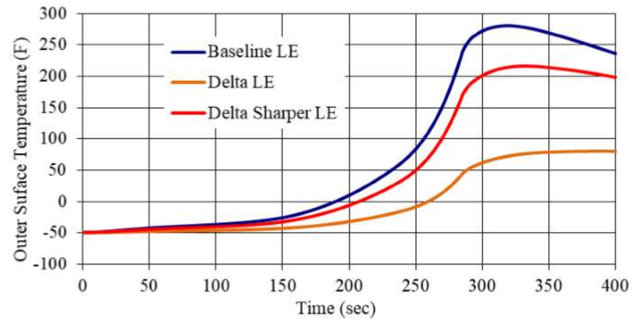

FIGURE 19 - Wing Leading Edge Outer Surface Temperature Time Histories with Different Configurations

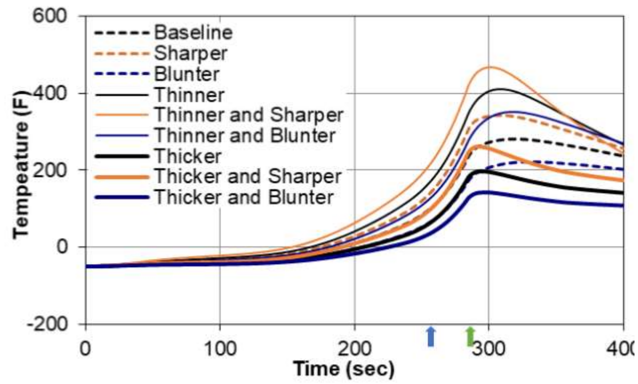

FIGURE 20 - Alternative Leading Edge Wing Thickness and Radius Temperature Time Histories

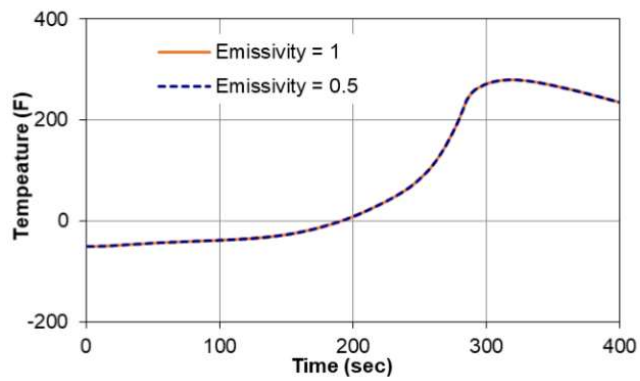

FIGURE 21 - Effect of Emissivity on Leading Edge Wing Temperature history

FIGUREs 22 and 23 shows the effect of changing the thickness away from the baseline.

Unsurprisingly increasing the thickness decreases the temperature and decreasing thickness increases temperature. The difference of changing the thickness by 0.010-in shows a modest change in temperature at t = 308-sec of about 30°F.

For the delta wing case a similar trend to that of FIGURE 22 and 23 is seen in FIGURE 24; the temperature decreases further along the chord. This case shows a similar temperature to the baseline for the low percent chord, < 40%, with the exception of the leading edge which is the sharp LE.

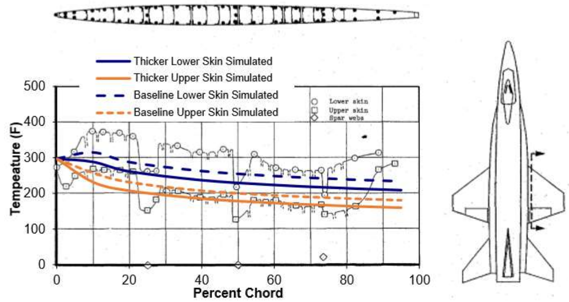

FIGURE 22 - Chordwise Temperature Distribution at t=308-sec for the Root Section, New Thicker Skin Thickness = 0.080-in

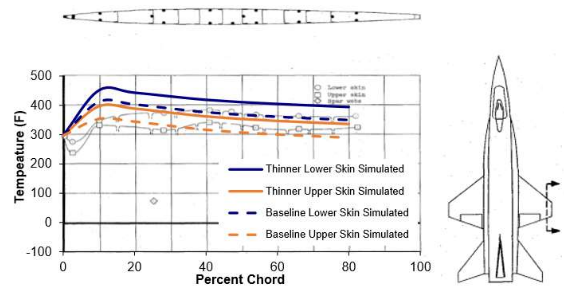

FIGURE 23 - Chordwise Temperature Distribution at t=308-sec for the Root Section, New Thinner Skin Thickness = 0.040-in

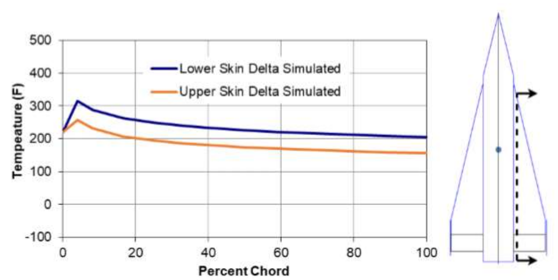

FIGURE 24 - Chordwise Temperature Distribution at t=308-sec for the Root Section of Delta Wing Configuration, Skin Thickness = 0.070-in

V.Conclusions

Hypersonic aircraft, even more so than conventional aircraft, express the adage that "everything effects everything."

In this paper, we demonstrate how a mission based trajectory / aerothermodynamic model can be used to assess detail (radius, emissivity and local parts thickness) as well as large-scale conceptual (alternative sweep / planform) changes to a high-speed aircraft configuration without the need for a "water-tight" CFD style geometry.

The results of this simulation as applied to the baseline X-15 geometry generally matches published data. Perturbations to the design may make regions of the airframe either hotter or cooler, with favorable or unfavorable impacts to the airframe materials design strategy.

Application of this tool to other candidate geometries can help support design trades and preliminary thermal protection system design strategies for a wide variety of future applications.

Acknowledgements

This research was supported in part by an appointment to the Postgraduate Research Participation Program at the U.S. Air Force Institute of Technology, administered by the Oak Ridge Institute for Science and Education through an interagency agreement between the U.S. Department of Energy and AFIT.

References

[1] Office of Unmanned Vehicles, "Flight Test Results from the Entry and Landing of the Space Shuttle Orbiter for the First Twelve Orbital Flights," AFFTC-TR-85-11, 1985.

[2] Griffin, J. A. and Takahashi, T.T., “Aero-Spaceplane Mission Performance Estimations Incorporating Atmospheric Control Limits,” AIAA 2022-3656, 2022.
[3] Griffin, J. A. , Takahashi, T.T. and Rodi, P.E. , “Aerothermodynamic Modeling for a “Mission Code” Approach to Hypersonic Flight,” AIAA 2022-3657, 2022.
[4] Hague, D.S., and Rozendaal, H.L., “NSEG – A Segmented Mission Analysis Program for Low and High Speed Aircraft. Volume I – Theoretical Development.” NASA Contractor Report 2807, August 1977.
[5] Hague, D.S., and Rozendaal, H.L., “NSEG – A Segmented Mission Analysis Program for Low and High Speed Aircraft. Volume II – Program Users Manual.” NASA Contractor Report 2808, September 1977.
[6] Hague, D.S., and Rozendaal, H.L., “NSEG – A Segmented Mission Analysis Program for Low and High Speed Aircraft. Volume III – Demonstration Problems.” NASA Contractor Report 2809, September 1977.
[7] Rutowski, E., “Energy Approach to the General Aircraft Performance Problem.” Journal of the Aeronautical Sciences, March 1954, pp.187-195.
[8] Takahashi, T.T., Aircraft Performance and Sizing, Volume I: Fundamentals of Aircraft Performance, Momentum Press, New York, 2016.
[9] Takahashi, T.T., Aircraft Performance and Sizing, Volume II: Applied Aerodynamic Design, Momentum Press, New York, 2016.
[10] Takahashi, T.T., “Optimal Climb Trajectories Through Explicit Simulation,” AIAA 2015-2701, 2015.
[11] Takahashi, T.T. and Sobester, A., “Climb Performance Anomalies in ‘Real’ Atmospheric Conditions,” AIAA 2019-3271, 2019.
[12] Anon.,"U.S. Standard Atmosphere, 1976," NASA-TM-X-74335, October 1976.
[13] Bertin, J.J., Hypersonic Aerothermodynamics, AIAA, Reston, VA, 1993.
[14] Ames Research Staff, “Equations, Tables, and Charts for Compressible Flow”, NACA Report 1135, 1953.
[15] Moeckel, W.E. and Weston, K.C. “Composition and Thermodynamic Properties of Air in Chemical Equilibrium,” NASA TN-4265, April 1958.
[16] Anderson, J.D., Hypersonic and High-Temperature Gas Dynamics, *3rd Edition,* AIAA, Reston, VA, 2019.
[17] Reed, R.D., and Watts J.D., “Skin and Structural Temperatures Measured on the X-15 Airplane During a Flight to a Mach Number of 3.3.” NASA TM-X-468, January 1961.
[18] Maher, J.F, Ottinger, C.W., and Capasso, V.N., “YLR99RM-1 Rocket Engine Operating Experience in the X-15 Aircraft,” NASA TN-D-2391, July 1964.